Inorganic Chemistry

Article

pubs.acs.org/IC

Crystal Structure, Exogenous Ligand Binding, and Redox Properties of an Engineered Diiron Active Site in a Bacterial Hemerythrin

Yasunori Okamoto,[†] Akira Onoda,*[,†] Hiroshi Sugimoto,[‡] Yu Takano,[§] Shun Hirota,[∥] Donald M. Kurtz, Jr.,[#] Yoshitsugu Shiro,[‡] and Takashi Hayashi*[,†]

[†]Department of Applied Chemistry, Graduate School of Engineering, Osaka University, Suita, Osaka 565-0871, Japan

[‡]Biometal Science Laboratory, RIKEN SPring-8 Center, Sayo, Hyogo 679-5148, Japan

[§]Institute for Protein Research, Osaka University, Suita, Osaka 565-0871, Japan

[∥]Graduate School of Materials Science, Nara Institute of Science and Technology, Ikoma 630-0192, Japan

[#]Department of Chemistry, University of Texas at San Antonio, San Antonio, Texas 78249, United States

Supporting Information

ABSTRACT: A nonheme diiron active site in a 13 kDa hemerythrin-like domain of the bacterial chemotaxis protein DcrH-Hr contains an oxo bridge, two bridging carboxylate groups from Glu and Asp residues, and five terminally ligated His residues. We created a unique diiron coordination sphere containing five His and three Glu/Asp residues by replacing an Ile residue with Glu in DcrH-Hr. Direct coordination of the carboxylate group of E119 to Fe2 of the diiron site in the I119E variant was confirmed by X-ray crystallography. The substituted Glu is adjacent to an exogenous ligand-accessible tunnel. UV−vis absorption spectra indicate that the additional coordination of E119 inhibits the binding of the exogenous ligands azide and phenol to the diiron site. The extent of azide binding to the diiron site increases at pH ≤ 6, which is ascribed to protonation of the carboxylate ligand of E119. The diferrous state (deoxy form) of the engineered diiron site with the extra Glu residue is found to react more slowly than wild type with O_2 to yield the diferric state (met form). The additional coordination of E119 to the diiron site also slows the rate of reduction from the met form. All these processes were found to be pH-dependent, which can be attributed to protonation state and coordination status of the E119 carboxylate. These results demonstrate that modifications of the endogenous coordination sphere can produce significant changes in the ligand binding and redox properties in a prototypical nonheme diiron-carboxylate protein active site.

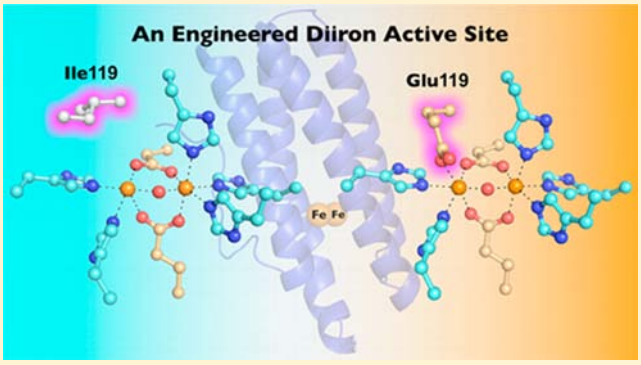

INTRODUCTION

Nonheme diiron-carboxylate active sites in proteins are involved in diverse reactions with O_2.[1−12] Hemerythrin (Hr), first identified in a limited number of marine invertebrates, is the only diiron-carboxylate protein known to reversibly bind O_2. Members of the Hr family contain a diiron site in which the two irons are linked with a μ-oxo/hydroxo bridge and two bridging carboxylate groups provided by Glu and Asp residues, as shown in Figure 1. The coordination spheres are completed by five terminal His residues, three for the six-coordinate iron (Fe1) and two for the five-coordinate iron (Fe2), the latter of which binds the O_2.

The factors influencing the diverse O_2 reactivities of seemingly similar nonheme diiron-carboxylate active sites in proteins are still incompletely understood. One approach to probing these factors is reengineering the function of these diiron sites. However, only a few such studies have been reported.[13−16] Engineered variants of O_2-binding pocket residues in inverterbrate Hrs show altered O_2 binding properties.[17,18] The replacement of Leu98 (which is located near the diiron site) with Tyr was found to generate new hydrogen-bonding interaction with Fe2-bound O_2.[19] As a target protein for engineering diiron-carboxylate coordination spheres, we selected the 13-kDa Hr-like domain of the bacterial chemotaxis protein *Desulfovibrio* chemoreceptor H (DcrH-Hr). DcrH-Hr contains the characteristic coordination sphere of Hrs shown in Figure 1 and shows the characteristic spectroscopic properties of the diiron site.[20] The crystal structure of DcrH-Hr revealed the existence of a larger ligand-accessible tunnel than that of invertebrate Hrs.[21] The diiron sites in invertebrate Hrs are not known to bind exogenous ligands containing more than three non-hydrogen atoms. However, the ligand-accessible tunnel of DcrH-Hr allows binding of relatively large exogenous ligands, such as phenol, to the diiron site.[20] The ability of the active site to accommodate larger and potentially oxidizable substrates also makes DcrH-Hr an attractive choice. We have previously reported that the larger exogenous ligand-accessible

Received: June 26, 2013
Published: November 4, 2013

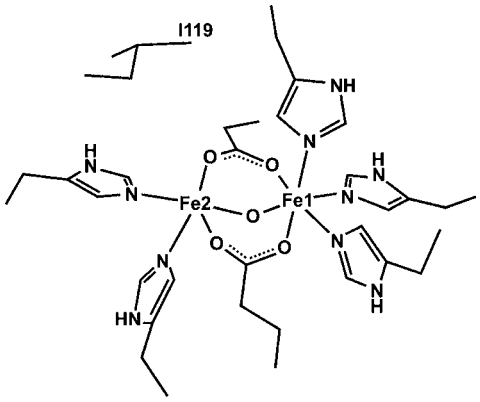

Figure 1. Schematic structure of the diiron active site and pocket Ile119 of DcrH-Hr.

tunnel accelerates O_2 binding and autoxidation and may contribute to stabilization of the mixed-valent states of the diiron site relative to invertebrate Hrs.[22] As a first trial on engineering the diiron coordination sphere in DcrH-Hr, we focused on Ile119, a conserved residue that lines the exogenous ligand-accessible tunnel and is positioned close to the diiron site (Figure 1). We substituted a Glu residue at this position with the expectation that it would bind directly to the diiron site in a pH-dependent manner and thereby modulate its ligand binding and redox chemistry. Here, we report the crystal structure, ligand binding properties, and redox properties of the diiron site in the I119E DcrH-Hr variant.

EXPERIMENTAL SECTION

Materials. Oligonucleotides were obtained from Invitrogen, Inc. Restriction enzymes were obtained from Takara Bio Inc. Nucleotide sequences were determined by FASMAC Co., Ltd. or the University of Texas Health Science Center, San Antonio Nucleic Acids Core Facility. All reagents of the highest guaranteed grade were purchased and used as received unless otherwise noted. Sodium azide-1-^{15}N was purchased from Isotech Laboratories Inc. Distilled water was demineralized by a Barnstead NANOpure DIamond apparatus.

Instruments. Purification of the proteins was performed at 4 °C using a GE Healthcare ÄKTA purifier system. UV−vis absorption spectra were obtained on a Shimadzu UV-3150 double-beam spectrophotometer equipped with a thermostatted cell holder (±0.1 °C) or on a Shimadzu BioSpec-nano spectrophotometer. The pH values were monitored with a Horiba F-52 pH meter.

Protein Overexpression. The expression plasmids of His-tagged wild-type DcrHr (WT) and tag-free recombinant DcrH-Hr were prepared by previously described procedures.[22] Plasmids containing the gene encoding the I119E variant DcrH-Hr (I119E) were constructed by a "round-the-horn" site-directed mutagenesis protocol using the expression plasmids for wild-type DcrH-Hr as a template. The forward primer overlapping the Ile119 codon, 5′-GAAATGAAA-GAAGACAAAAAATATGAAGCGTATCTGCG-3′, where the variant codons are underlined, and reverse primer 5′-GTGGTTGACCAGC-CAGTCAA-3′ were used for the tag-free I119E. In a similar way, the forward primer 5′-CATGAAATGAAGGAGGACAAGAAGTAC-GAGGCGTACTTGCGCG-3′ and the reverse primer 5′-GTTCAC-CAGCCAGTCGACGAGTCCG-3′ were used for the His-tagged I119E. Each of the expression plasmids of His-tagged WT, His-tagged I119E, and tag-free I119E were transformed into *E. coli* BL21(DE3). Twenty-milliliter cultures of the transformed cells in Luria−Bertani broth (LB) containing 50 μg/mL ampicillin were incubated overnight at 37 °C. The 20 mL cultures were used to inoculate 1 L batches of LB containing ampicillin (50 mg) and 1% (w/v) glucose. The inoculated 1 L cultures were incubated aerobically with vigorous shaking at 37 °C. When the cultures' OD_{600} reached 1.0, isopropyl β-D-1-thiogalactopyranoside was added to a final concentration of 0.4 mM to induce protein expression. Ammonium iron(II) sulfate (30 mg) was also added to facilitate incorporation of iron into the expressed protein. The cultures were incubated at 25 °C overnight with shaking, and the cells were harvested by centrifugation.

The harvested cells from 10 L of culture were resuspended in 200 mL of 50 mM 3-(*N*-morpholino)propanesulfonic acid (MOPS) (pH 7.3) and lysed by sonication. Cell debris was removed from the lysate by centrifugation at 20000*g* for 60 min, and the yellow supernatant was loaded onto a column packed with 10 mL of TALON metal affinity resin (Clontech Laboratories, Inc.) that was pre-equilibrated in 50 mM MOPS buffer (pH 7.3) containing 250 mM NaCl. After the column was washed with 50 mL of washing buffer (50 mM MOPS (pH 7.3), 10 mM imidazole, 250 mM NaCl), the His-tagged WT or I119E was eluted as a yellow-green band with 50 mL of elution buffer (50 mM MOPS (pH 7.3), 0.5 M imidazole, 0.5 M NaCl). The collected fraction was buffer-exchanged into imidazole-free 50 mM MOPS (pH 8.0) buffer. The iron content in the purified protein was quantified by ferrozine iron analysis.[23] The His-tagged WT and I119E proteins purified in this fashion were quantified by Bradford assay and the absorption in the met form and used for all experiments except for protein crystallography.

For protein crystallography, cells were harvested from 4 L of culture expressing the tag-free I119E. These cells were resuspended in 100 mL of 50 mM MOPS (pH 7.3) and lysed by freeze−thaw cycles. The lysate was treated with benzonase nuclease (Novagen) (250U) for 40 min at 25 °C. The supernatant from centrifugation of the treated lysate was diluted 10-fold with 50 mM MOPS (pH 7.3). The diluted solution was loaded onto an anion-exchange column packed with DEAE Sepharose Fast Flow resin (GE Healthcare), which was pre-equilibrated in 50 mM MOPS (pH 7.3). The flow-through fraction containing I119E was collected and concentrated to 5 mL using an Amicon stirred ultrafiltration cell with a 10 kDa molecular weight cutoff membrane (Millipore). The sample solution was loaded onto a HiTrap Q anion-exchange column, and a flow-through fraction was collected. The sample fraction was loaded onto a Sephacryl S-200 column (GE Healthcare) equilibrated in the same buffer.

Preparation of the Met Form. The purified preparations of WT and I119E were treated with at least 10 equiv of potassium ferricyanide at 4 °C for 16 h, and the resulting samples were purified using a HiTrap desalting column (GE Healthcare) equilibrated with 50 mM MES (pH 6.0), 50 mM HEPES (pH 7.0), and 50 mM HEPES (pH 8.0).

Preparation of the Deoxy Form and Reaction with O_2. The purified WT or I119E in buffers (50 mM 2-(*N*-morpholino)-ethanesulfonic acid (MES) (pH 6.0), 50 mM 4-(2-hydroxyethyl)-1-piperazineethanesulfonic acid (HEPES) (pH 7.0), or 50 mM HEPES (pH 8.0)) was anaerobically reduced to the deoxy form by addition of at least 20 equiv of sodium dithionite and 5 equiv of methylviologen at room temperature. The solution was incubated for 3 h in a glovebox under an N_2 atmosphere. The resulting solution was immediately used for the O_2 reaction kinetics experiments after passing over a HiTrap desalting column (GE Healthcare) equilibrated with air-saturated 50 mM HEPES (pH 7.0).

Dissociation Constants for Azide Binding. UV−vis absorption spectra of the azide adduct of met-WT and met-I119E were obtained after the addition of sodium azide (0 to 3 equiv to met-WT and 0 to 3000 equiv to met-I119E) to a 100 μM solution of proteins in 50 mM HEPES (pH 7.0) or 50 mM MES (pH 6.0) and a 12 h incubation at 4 °C. The concentrations of the azide-free and azide-bound met-WT were determined from the absorbances at 455 nm, respectively. The concentration of the azide-free and azide-bound met-I1119E was determined from the absorption at 451 nm, respectively. The K_d values were evaluated by fitting the experimentally obtained concentration to the following equation: K_d = [azide-free protein][azide]/[azide-bound protein].

Resonance Raman Spectroscopy. Resonance Raman scattering was excited at 488.0 nm with an Ar^+ laser (Spectra Physics, 2017) and detected with a CCD (Princeton Instruments) attached to a triple polychrometer (JACSO, NR-1800). The slit width was set to 200 μm.

dx.doi.org/10.1021/ic401632x | *Inorg. Chem.* 2013, 52, 13014−13020

The laser power was 100 mW at the sample point. The spectra were collected at room temperature with a spinning cell. The concentration of all samples was maintained at 1 mM. Toluene and acetone were used as references. The accuracy of the peak positions of the Raman bands was ±1 cm^{-1}.

Crystallization and Structural Analysis. Crystals of I119E in the met form (met-I119E) were grown by a batch method. The protein solution (50 mg/mL) in 50 mM MOPS pH 7.0 in a 1.5 mL microtube was kept at 4 °C for 2 days. Crystals of met-I119E belong to space group $P2_12_12_1$ with one monomer per asymmetric unit. Crystals were cryo-protected for X-ray diffraction data collection by soaking in mixed oil [66.5% (v/v) Paratone-N, 28.5% (v/v) paraffin oil, 5.0% (v/v) glycerol] for 2 min,[24] and the buffer solution surrounding the crystal was removed. The crystal was then picked up in a cryoloop and frozen in liquid nitrogen. X-ray diffraction data were collected on the BL41XU beamline at the SPring-8 synchrotron radiation facility. The data were integrated and scaled using the program HKL2000[25] and further processed using the CCP4 software package.[26] The initial phases were obtained by the molecular replacement method using the Molrep program.[27] The reported structure of WT in the met form (met-WT) (PDB code 3AGT) was used as a search model. The model was refined with multiple rounds of manual rebuilding using Coot,[28] and crystallographic refinement by PHENIX[29] at 1.8 Å resolution. The simulated annealing algorithm was used in the initial stage of structure refinement. The data collection and refinement statistics are listed in Table 1. Figures depicting the structure were prepared with PYMOL (http://www.pymol.org).[30] The atomic coordinates and structure factors have been deposited into the Protein Data Bank (http://www.rcsb.org/PDB code 3WAQ).

Table 1. Statistics of X-ray Crystallographic Data and Structure Refinement

Data Collection	
beamline	BL41XU
wavelength (Å)	1.0000
resolution (Å)[a]	20−1.8 (1.86−1.8)
space group	$P2_12_12_1$
cell dimensions (Å)	
a	31.0
b	50.9
c	76.7
total reflns	79 971
unique reflns	11 822
R_{sym} (%)[a,b]	6.1 (27.9)
completeness (%)[a]	99.8 (99.3)
$I/\sigma(I)$[a]	25.1 (4.9)
redundancy[a]	6.2 (6.8)
Refinement	
resolution range (Å)	20−1.8
R/R_{free} factor (%)	20.7/26.1
rms deviation	
bond lengths (Å)	0.015
bond angles (deg)	1.3
Ramachandran (%)	
most favored	94.1
additional allowed	5.2
generously allowed	0.7

[a]Numbers in parentheses are for the highest resolution shell. [b]$R_{sym} = \sum_{hkl}\sum_i|I_i(hkl) - \langle I(hkl)\rangle|/\sum_{hkl}\sum_i I_i(hkl)$ where $\langle I(hkl)\rangle$ is the average intensity of the *i* observations. $R = \sum_{hkl}|F_{obs}(hkl) - F_{calc}(hkl)|/\sum_{hkl}F_{obs}(hkl)$, where F_{obs} and F_{calc} are observed and calculated structure factors, respectively. R_{free} was calculated with 5% of the reflections.

RESULTS AND DISCUSSION

Characterization of the I119E Variant. The His-tagged I119E migrated as a single band in sodium dodecyl sulfate polyacrylamide gel electrophoresis with a molecular weight of 15 kDa (Figure S1). The tag-free I119E migrated at a molecular weight of ∼13 kDa as expected for the absence of the tag (Figure S2). The purified preparation of I119E contained approximately 1.7 iron atoms per molecule of protein. The I119E was treated with potassium ferricyanide to fully oxidize the iron to the diferric state (met form). The UV−vis absorption spectrum of the met-I119E exhibited maxima at 325 and 370 nm. The spectrum closely resembles that of WT, and these two absorption features are assigned as the oxo-ligand-to-ferric charge transfer transitions characteristic of the oxo/dicarboxylato-bridged diferric sites in Hrs (Figure 2).[2,20,31] These characteristic absorption features suggest that the diiron bridging ligands are conserved in met-I119E.

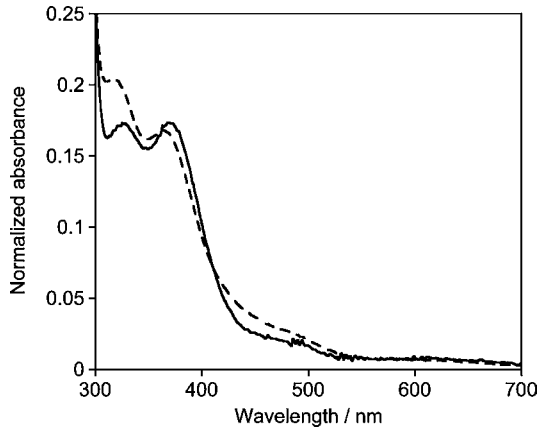

Figure 2. UV−vis absorption spectra of met-WT (dashed line) and met-I119E (solid line) DcrH-Hrs in 50 mM HEPES (pH 7.0).

Crystal Structure. The X-ray crystal structure of met-I119E was determined and refined at a 1.8 Å resolution (Figure 3a, Table 1). The two iron atoms within the four-helix bundle are 3.2 Å apart and contain a bridging oxygen atom with an Fe1−μO−Fe2 angle of 122°. The same five terminally ligated histidine residues and two bridging carboxylate-containing residues (Asp and Glu) as in WT provide ligands to the diiron site in I119E. This diiron site geometry is, thus, very similar to that in WT and invertebrate Hrs (Table S1). A unique feature of the I119E structure is that the carboxyl group of E119 coordinates to the Fe2 atom in place of an exogenous chloride in WT (Figure 3b). The Fe2−Oε1(E119) distance is 2.1 Å, and the Fe2−Oε1−Cδ(E119) angle is 102°. The noncoordinated carboxylate oxygen atom of E119 forms a hydrogen bond with the N1 atom of W114 that lines the ligand-accessible tunnel. This interaction causes the side chain of W114 to rotate relative to its position in WT with an increase of the χ^2 angle of ca. 180° (Figure S3). The rotation of the W114 residue is accompanied by a small kink in the N-terminal region of helix 4 and the adjacent C-terminal region of helix 3; the structure of the N-terminal region of helix 1 is also slightly perturbed. A larger structural perturbation occurs in residues of the intervening loops between the helices, as indicated by the differences in the ϕ and φ dihedral angles between WT and I119E (Figure S4). The ligand-accessible tunnel structure leading to the diiron site is relatively unperturbed by the I-to-E

dx.doi.org/10.1021/ic401632x | Inorg. Chem. 2013, 52, 13014−13020

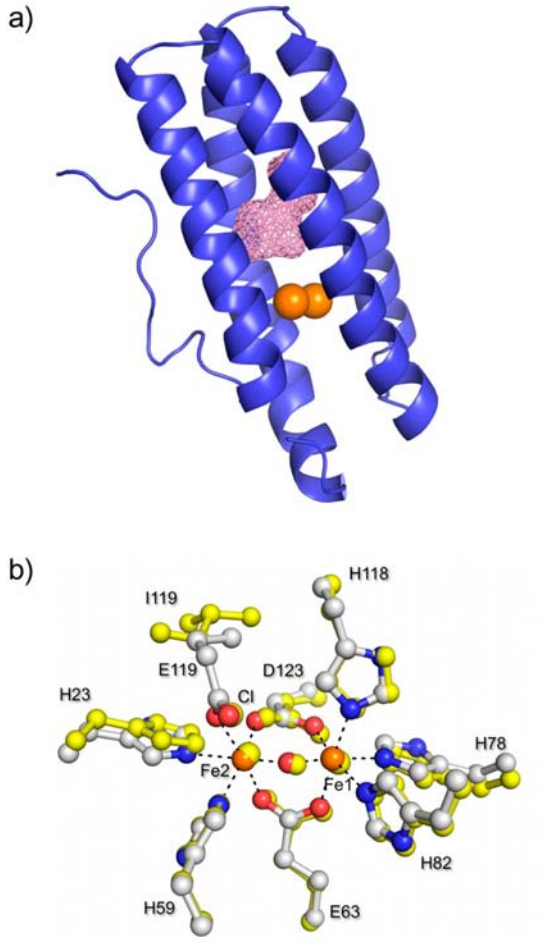

Figure 3. (a) Protein backbone and diiron site structure of met-I119E. The pink grid surface represents the ligand-accessible tunnel. (b) Superimposition of the diiron site structure of I119E (iron in orange, carbon in white, oxygen in red, and nitrogen in blue) with that of WT (yellow).

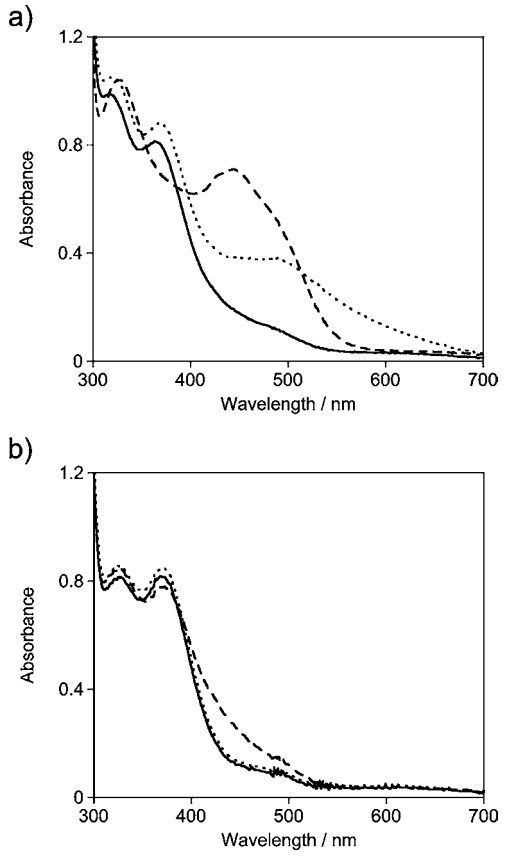

Figure 4. UV–vis absorption spectra of (a) met-WT and (b) met-I119E in the presence of exogenous ligands in 50 mM HEPES (pH 7.0). Proteins (150 μM) in the absence of ligands (solid lines) and in the presence of either 7.5 mM NaN_3 (dashed lines) or 7.5 mM phenol (dotted lines). Spectra were obtained after 12 h of incubation at 4 °C.

substitution, except that the exogenous ligand coordination site on Fe2 is occupied by the E119 carboxylate (Figure 3 and Figure S5).

Exogenous Ligand Binding Properties. The UV–vis absorption spectral changes of met-WT and met-I119E that occur upon addition of the exogenous ligands, azide and phenolate, are shown in Figure 4. Addition of 50 equiv of azide to met-WT induced a spectrum characteristic of the Hr–azide adduct with maxima at ~320 and 443 nm (Figure 4a),[20] whereas the same excess of azide added to met-I119E induced only minor perturbations in its absorption spectrum (Figure 4b). Azide-induced absorption changes for met-I119E were observed only at large excesses (1000 equiv) of azide (Figure S6). Differing characteristics of phenol binding to met-WT and met-I119E are also readily apparent from their respective UV–vis absorption spectra. Addition of phenol to met-WT induces formation of a characteristic absorption band at 500 nm due to the binding of phenol to the diiron site (Figure 4a).[20] However, no spectral changes were observed upon the addition of excess phenol to met-I119E (Figure 4b). Thus, the introduction of the E119 carboxylate ligand apparently impedes (azide) or prevents (phenol) binding of exogenous ligands to the diiron site.

The spectrum of the azide adduct of met-WT was found to be independent of pH values between 8 and 6 (Figure 5). In the case of the azide-treated met-I119E, the intensity of the absorption at 425 nm increased with a decrease in pH from 8 to 6. Moreover, the K_d value of met-WT at neutral pH was found to be less than 1 μM and does not vary between pH 6.0 and 7.0.[32] The K_d value of met-I119E clearly depends on the pH values, and the affinity is much lower than that of met-WT: 16 mM at pH 7.0 and 1.9 mM at pH 6.0 (Figure S7). These findings are consistent with protonation of the E119 carboxylate and its dissociation from Fe2 under acidic conditions.

Resonance Raman Spectroscopy. The structures of the diiron site of met-I119E and its azide adduct were analyzed by resonance Raman (rR) spectroscopy, which has been previously used as a selective probe of the oxo-bridged diiron(III) unit,[31] including that in WT DcrH-Hr.[20] The rR spectra of met-WT are shown in Figure 6. The major peak at 500 cm^{-1} was previously assigned to a symmetric Fe–μ-O–Fe stretching vibrational mode, which is characteristic of the bent Fe–μ-O–Fe geometry in dicarboxylate-bridged Fe^{III}–μ-O–Fe^{III} complexes (Figure 6a).[20,31] The major peak at 504 cm^{-1} in the rR spectrum of met-I119E can therefore be assigned to the same Fe–μ-O–Fe vibrational mode (Figure 6b). These results indicate that the bent Fe–μ-O–Fe unit is conserved in met-I119E. The rR spectrum of the azide adduct of met-WT revealed three major peaks at 499, 372, and 297 cm^{-1} (Figure 6c). The two peaks at 499 and 297 cm^{-1} were previously assigned to symmetric and bending Fe–μ-O–Fe vibrational modes, respectively, and the peak at 372 cm^{-1} was assigned to

dx.doi.org/10.1021/ic401632x | Inorg. Chem. 2013, 52, 13014–13020

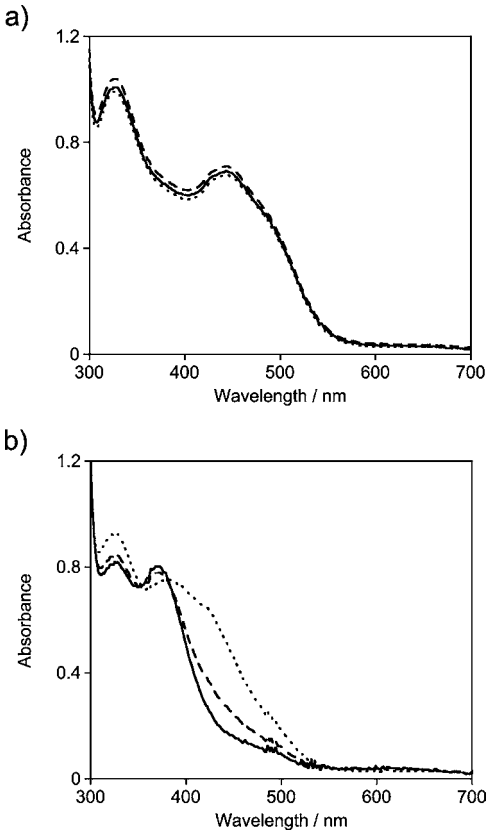

Figure 5. pH dependence of the UV−vis absorption spectra of azide-bound (a) met-WT and (b) met-I119E. Protein samples (150 μM) were in 50 mM HEPES (pH 8.0) (solid lines), 50 mM HEPES (pH 7.0) (dashed lines), and 50 mM MES (pH 6.0) (dotted lines). Spectra were obtained after 12 h incubation at 4 °C.

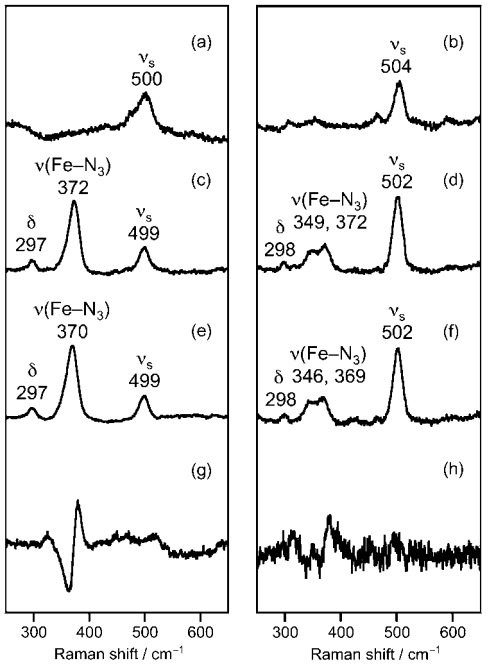

Figure 6. Resonance Raman spectra of met-WT (left) and met-I119E (right): (a and b) in the absence of azide, (c and d) in the presence of 50 mM $Na^{14}N_3$, and (e and f) in the presence of 50 mM $Na^{15}N_3$. (g and h) $^{15}N_3/^{14}N_3$ difference spectra. The laser excitation wavelength was 488 nm. Protein samples (1 mM) were in 50 mM HEPES (pH 7.0) and were kept at room temperature. Peaks are labeled according to their vibrational assignments, as described in the text.

Scheme 1

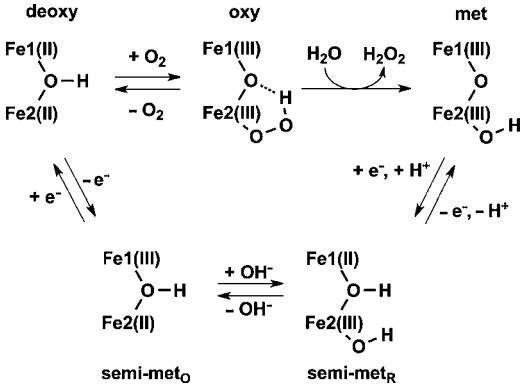

the Fe−N_3 stretching vibration.[20] In contrast, the rR spectrum of the azide adduct of met-I119E shows four peaks at 502, 372, 349, and 298 cm^{-1} (Figure 6d). The two peaks at 372 and 349 cm^{-1} were assigned as Fe−N_3 stretching vibrations by $^{14}N_3^-/^{15}N_3^-$ isotope labeling experiments (Figure 6e, f, g, and h). These intensities are weaker relative to the intensity of the 372 cm^{-1} peak in the azide-bound met-WT rR spectrum, presumably because of the lower affinity of azide for the diiron site, as determined by the UV−vis absorption spectra. This conclusion is further supported by the pH dependence of the rR spectra (Figure S8), which parallels that of the UV−vis absorption spectra shown in Figure 5. The down-shifted Fe−N_3 vibrational mode at 349 cm^{-1} could be due to either steric or electronic (e.g., hydrogen bonding) alterations of the azide coordination geometry caused by the E119 side chain.

Reaction with O_2. The reactions of the deoxy WT and I119E with O_2 were compared to determine the influence of the I-to-E substitution. The kinetics of the reaction of O_2 with deoxy WT was previously described according to Scheme 1.[22] Fully reduced diferrous (deoxy) proteins were treated with O_2 by passing the proteins through a HiTrap desalting column equilibrated with air-saturated buffer. This treatment of the deoxy WT immediately provided a UV−vis absorption spectrum with a maximum at 500 nm characteristic of the oxy form (Figure 7a). This characteristic absorption then decreased concomitant with an increase of the absorption at 392 nm, indicating autoxidation to the met form.[22] The analogous O_2 exposure for deoxy I119E shows no spectral changes at 500 nm that could indicate an O_2 adduct; only the smooth development of the met spectrum occurred over 1 h (Figure 7b). This formation of the met spectrum for I119E was approximately 3-fold slower than that for WT. According to Scheme 1, this observation can be attributed mainly to deceleration of the binding of O_2 relative to autoxidation. In addition, the conversion from the deoxy to the met form in I119E was found to be accelerated at pH 6 (Figure S9), which, as for the pH-dependent azide binding, can be attributed to protonation and dissociation of the carboxylate ligand.[33]

Reduction of the Met Form to the Semi-met_R Form. To understand how the coordination of E119 affects the redox properties of the diiron site, outer-sphere one-electron reduction from the met form [$Fe1^{III}Fe2^{III}$] to the semi-met_R form, [$Fe1^{II}Fe2^{III}$] (Figure S10), was monitored upon addition of 4-aminophenol, which has a reduction potential of 0.314 V

dx.doi.org/10.1021/ic401632x | Inorg. Chem. 2013, 52, 13014−13020

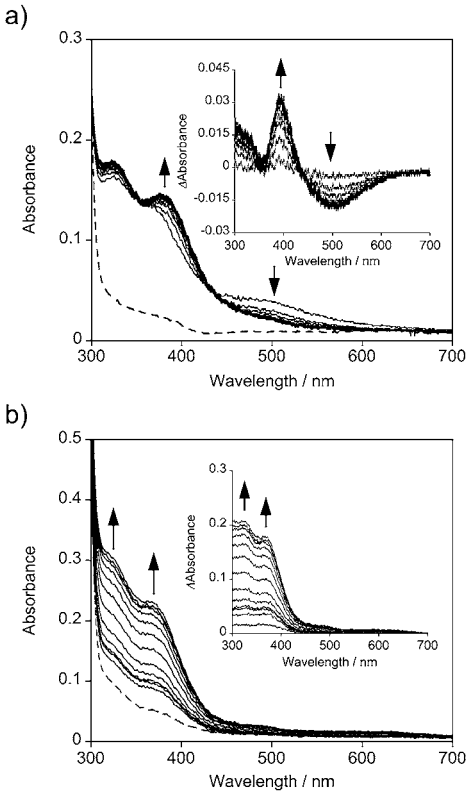

Figure 7. Spectral changes observed after mixing the deoxy forms of (a) WT and (b) I119E with air-saturated buffer recorded at 5 min intervals to 60 min. The dashed curves are the spectra of the deoxy form. [Proteins] = 50 μM, 50 mM HEPES (pH 7.0) at 20 °C. Inset: Difference absorption spectral time course (a) subtracting the oxy spectrum from each subsequent spectrum and (b) subtracting the deoxy spectrum from each subsequent spectrum.

(vs SHE).[34,35] The met form of the proteins (100 μM) was mixed with 4-aminophenol (5 mM) under anaerobic conditions at pH 6.0 or 8.0 (Figure S11). Addition of 4-aminophenol to the proteins caused a decrease in the absorption around 370 nm, resulting in the spectrum expected for the semi-met$_R$ form.[22,36] The reduction of met-I119E is much slower than that of met-WT. The reduction rate of met-WT is independent of pH values (pH 6.0−8.0), whereas the reduction rate of met-I119E at pH 8.0 is further decelerated relative to that of the same reaction at pH 6.0. The reduction rate from the met form to the semi-met$_R$ form for I119E was also found to be slower than WT using 1 equiv of the stronger reducing agent, sodium dithionite (Figure S12). The slower reduction of I119E could be construed as either kinetic or thermodynamic stabilization of Fe2 in the Fe^{III} state by E119 carboxylate coordination.[37]

CONCLUSIONS

To engineer the coordination environment of the diiron site in DcrH-Hr, we replaced a conserved isoleucine residue lining the exogenous ligand-accessible tunnel with a glutamic acid residue. The diiron structure of the met form is conserved in the I119E variant, with the exception that the E119 carboxylate terminally coordinates to the Fe2 atom of the diferric site. The newly introduced coordination between the Glu residue and Fe2 inhibits exogenous ligand binding and slows autoxidation of the deoxy and reduction of the met form. These processes clearly depend on pH, which can be attributed to the protonation and ligation state of the E119 carboxylate. The results demonstrate that modification of a small residue located in the second coordination sphere in a prototypical nonheme diiron-carboxylate site can produce significant influences on ligand binding and redox properties. Further engineering to convert the DcrH-Hr diiron site into an active catalyst is now in progress.

ASSOCIATED CONTENT

Supporting Information

SDS-PAGE analyses for purification, a figure showing ϕ and φ dihedral angles between met-WT and met-I119E, the superimposed structures showing substrate-access tunnels of met-WT and met-I119E, UV−vis absorption and rR spectra of the azide adduct of met-I119E, UV−vis absorption spectra of reductive titrations of met forms, optimized structures and calculated Gibbs free energy differences of the active site models, EPR spectra of semi-met$_R$-I119E. This material is available free of charge via the Internet at http://pubs.acs.org.

AUTHOR INFORMATION

Corresponding Authors

*E-mail: onoda@chem.eng.osaka-u.ac.jp (A.O.).
*E-mail: thayashi@chem.eng.osaka-u.ac.jp (T.H.).

Notes

The authors declare no competing financial interest.

ACKNOWLEDGMENTS

This work was financially supported by Grants-in-Aid for Scientific Research ((C), JSPS KAKENHI Grant Number 205590020, and Innovative Areas "Molecular Activation", area 2204, MEXT KAKENHI Grant Number 221050130). Y.O. appreciates support from Research Fellowship of JSPS and Global COE Program "Global Education and Research Center for Bio-environmental Chemistry" of Osaka University. D.M.K. acknowledges support from the National Institutes of Health (Grant R01 GM040388). The computations were performed using the Research Center for Computational Science, Okazaki, Japan.

REFERENCES

(1) Kurtz, D. M., Jr. *J. Biol. Inorg. Chem.* **1997**, *2*, 159−167.
(2) Kurtz, D. M., Jr. Dioxygen-Binding Proteins. In *Comprehensive Coordination Chemistry II*; McCleverty, J. A., Meyer, T. J., Eds.; Elsevier: Oxford, U.K., 2004; Vol. *8*, pp 229−260.
(3) Krebs, C.; Bollinger, J. M., Jr.; Booker, S. J. *Curr. Opin. Chem. Biol.* **2011**, *15*, 291−303.
(4) Kryatov, S. V.; Rybak-Akimova, E. V.; Schindler, S. *Chem. Rev.* **2005**, *105*, 2175−2226.
(5) Wilkins, P. C.; Wilkins, R. G. *Coord. Chem. Rev.* **1987**, *79*, 195−214.
(6) Stenkamp, R. E. *Chem. Rev.* **1994**, *94*, 715−726.
(7) Wallar, B. J.; Lipscomb, J. D. *Chem. Rev.* **1996**, *96*, 2625−2657.
(8) Tinberg, C. E.; Lippard, S. J. *Acc. Chem. Res.* **2011**, *44*, 280−288.
(9) Tomter, A. B.; Zoppellaro, G.; Anderson, N. H.; Hersleth, H.-P.; Hammerstad, M.; Røhr, Å. K.; Sandvik, G. K.; Strand, K. R.; Nilsson, G. E.; Bell, C. B., III; Barra, A.-L.; Blasco, E.; Pape, L. L.; Solomon, E. I.; Andersson, K. K. *Coord. Chem. Rev.* **2013**, *257*, 3−26.
(10) Nordlund, P.; Eklund, H. *Curr. Opin. Struct. Biol.* **1995**, *5*, 758−766.
(11) Fox, B. G.; Lyle, K. S.; Rogge, C. E. *Acc. Chem. Res.* **2004**, *37*, 421−429.
(12) Feig, A. L.; Lippard, S. J. *Chem. Rev.* **1994**, *94*, 759−805.

(13) Moënne-Loccoz, P.; Baldwin, J.; Ley, B. A.; Loehr, T. M.; Bollinger, J. M., Jr. *Biochemistry* **1998**, *37*, 14659−14663.
(14) Treffry, A.; Zhao, Z.; Quail, M. A.; Guest, J. R.; Harrison, P. M. *Biochemistry* **1997**, *36*, 432−441.
(15) Berthold, D. A.; Andersson, M. E.; Nordlund, P. *Biochim. Biophys. Acta* **2000**, *1460*, 241−254.
(16) Ajayi, W. U.; Chaudhuri, M.; Hill, G. C. *J. Biol. Chem.* **2002**, *277*, 8187−8193.
(17) Xiong, J.; Phillips, R. S.; Kurtz, D. M., Jr.; Jin, S.; Ai, J.; Sanders-Loehr, J. *Biochemistry* **2000**, *39*, 8526−8536.
(18) Farmer, C. S.; Kurtz, D. M., Jr.; Phillips, R. S.; Ai, J.; Sanders-Loehr, J. J. *J. Biol. Chem.* **2000**, *275*, 17043−17050.
(19) Farmer, C. S.; Kurtz, D. M., Jr.; Liu, Z. J.; Wang, B. C.; Rose, J.; Ai, J.; Sanders-Loehr, J. *J. Biol. Inorg. Chem.* **2001**, *6*, 418−429.
(20) Xiong, J.; Kurtz, D. M., Jr.; Ai, J.; Sanders-Loehr, J. *Biochemistry* **2000**, *39*, 5117−5125.
(21) Isaza, C. E.; Silaghi-Dumitrescu, R.; Iyer, R. B.; Kurtz, D. M., Jr.; Chan, M. K. *Biochemistry* **2006**, *45*, 9023−9031.
(22) Onoda, A.; Okamoto, Y.; Sugimoto, H.; Shiro, Y.; Hayashi, T. *Inorg Chem* **2011**, *50*, 4892−4899.
(23) Stookey, L. L. *Anal. Chem.* **1970**, *42*, 779−781.
(24) Sugahara, M.; Kunishima, N. *Acta Crystallogr. D* **2006**, *62*, 520−526.
(25) Otwinowski, Z.; Minor, W. *Methods Enzymol.* **1997**, *276*, 307−326.
(26) Collaborative Computational Project, Number 4 "The CCP4 suite, programs for protein crystallography". *Acta Crystallogr. D* **1994**, *50*, 760−763.
(27) McCoy, A. J.; Grosse-Kunstleve, R. W.; Adams, P. D.; Winn, M. D.; Storoni, L. C.; Read, R. J. *J. Appl. Crystallogr.* **2007**, *40*, 658−674.
(28) Emsley, P.; Cowtan, K. *Acta Crystallogr. D* **2004**, *60*, 2126−2132.
(29) Adams, P. D.; Afonine, P. V.; Bunkóczi, G.; Chen, V. B.; Davis, I. W.; Echols, N.; Headd, J. J.; Hung, L.-W.; Kapral, G. J.; Grosse-Kunstleve, R. W.; McCoy, A. J.; Moriarty, N. W.; Oeffner, R.; Read, R. J.; Richardson, D. C.; Richardson, J. S.; Terwilliger, T. C.; Zwart, P. H. *Acta Crystallogr. D* **2010**, *66*, 213−221.
(30) DeLano, W. L. *The PyMOL Molecular Graphics System*; DeLano Scientific: San Carlos, CA, 2008.
(31) Kurtz, D. M., Jr. *Chem. Rev.* **1990**, *90*, 585−606.
(32) The value is similar to the reported value of 1.0 μM for Hrs. Garbett, K.; Darnall, D. W.; Klotz, I. M. *Arch. Biochem. Biophys.* **1971**, *142*, 455−470.
(33) The half-lives of the autoxidation for WT at pH 7 and pH 8 are 5.3 and 22 min, respectively.
(34) Kano, K. *Rev. Polarogr.* **2002**, *48*, 29−46.
(35) Faiella, M.; Andreozzi, C.; de Rosales, R. T. M.; Pavone, V.; Maglio, O.; Nastri, F.; DeGrado, W. F.; Lombardi, A. *Nat. Chem. Biol.* **2009**, *5*, 882−884.
(36) The oxidation of 4-aminophenol was also determined by the absorption increase of the aminoindoaniline in the presence of *m*-phenylenediamine.
(37) We calculated the Gibbs free energy differences between the met and semi-met$_R$ for the WT and I119E diiron sites for the optimized structures of the diiron active sites (Figure S13). Each value for WT is lower than that estimated for I119E. It appears that the E119 carboxylate coordination has the effect of stabilizing the [Fe1^{III}Fe2^{III}] form (Table S3).